Front microrheology of the viscosity of blood infected by malaria

Author: Nil Masó Castro
Facultat de Física, Universitat de Barcelona, Diagonal 645, 08028 Barcelona, Spain.

Advisor: Aurora Hernández Machado, Hernando A. del Portillo

Abstract: We develop a mathematical model to characterize Newtonian and non-Newtonian fluids and compute their viscosity. Experimental data of mice blood infected by *Plasmodium yoelii* is analysed in order to obtain its viscosity. A comparison between different periods of infection is made with a view to determine viscosity changes throughout the disease advance. The results are also compared with non-infected human blood viscosity values to study how malaria affects the viscosity. Results successfully correlate with the already known viscoelastic changes of malaria-infected red blood cells.

I. INTRODUCTION

Microfluidics is the science that studies the behaviour of fluids at a very small scale, usually dealing with low Reynolds numbers. This allow us to get precise and accurate measurements with very low volumes of fluids. Hemorheology is the study of blood flow and its viscoelastic properties. Microfluidic devices are often needed in this field in order to study blood viscosity and its changes due to hematological disorders.

Nearly half of blood volume is red blood cells (RBCs), thus its viscosity will rely on the viscoelastic properties of these blood cells. More specifically, it depends on hematocrit (volume percentage of RBCs in blood), RBCs deformation and elasticity (which affect aggregation properties), and plasma viscosity (being the less prominent contribution) [1]. It also depends on the shear rate applied (the rate at which tangential force is applied), which changes the viscoelastic properties of RBCs and their aggregation.

Malaria is one of the most contracted parasite diseases worldwide, having more than 200 million cases in 2016 [2]. It is caused by parasites of the *Plasmodium* group that are transmitted by the bite of an infected *Anopheles* mosquito. Only a small fraction of victims die from malaria, the vulnerable population (elders and children) being the most endangered. For instance, *Plasmodium vivax* is associated with a greater risk of sever thrombocytopenia and sever anemia in infants [3].

When a *Plasmodium* parasite hosts a healthy RBC, the erythrocyte's viscoelastic properties change, modifying the whole blood viscosity. The infected RBCs (IRBCs) rigidity and flexibility changes depending on the *Plasmodium* specie infecting. This is experimentally shown elsewhere [4], which proves that as the parasite matured, *P. falciparum* IRBCs increased their rigidity whereas *P. vivax* IRBCs doubled their flexibility. Rigidity of the RBCs when infected by *P. falciparum* is also experimentally confirmed in [5]. It is also shown that *P. vivax* tends to increase the surface area of the RBC, which results in a higher flexibility [6].

A way to study blood infected by malaria is to first use mice blood, which is the aim of this study. The two most common species of *Plasmodium* in humans are *falciparum* and *vivax* but in order to study the effects on blood viscosity we can experiment with their equivalent *Plasmodium* species for mice, *P. chabaudi* and *P. yoelii*, respectively. This is a more ethical way to study these parasites, as direct infection of a human is not needed. Both *P. vivax* and *P. yoelii* exhibit tropism for reticulocytes (immature RBCs) and both tend to increase the flexibility of the RBCs.

II. MATHEMATICAL MODEL

As for any fluid, we need to derive the Navier-Stokes equation. This model works for any fluid not depending on the deformation history or the temperature (we will work at constant temperature). This includes Newtonian and non-Newtonian fluids. Considering a Ostwald-de Waele power law behaviour we can approximate the viscosity of the fluid η depending on the shear rate applied $\dot{\gamma}$:

$$\eta = m\dot{\gamma}^{n-1} \tag{1}$$

Here m is the flow consistency index and n is the power law exponent, which depends on the fluid behaviour. For Newtonian fluids n equals to 1, since viscosity doesn't depend on the shear rate applied. For non-Newtonian fluids n can be $n > 1$ for shear-thickening and $n < 1$ for shear-thinning fluids. Blood has a shear-thinning behaviour, so we will be dealing with values of $n < 1$.

The shear rate applied inside the microchannel can be approximated as:

$$\dot{\gamma} = \frac{\partial v_x}{\partial z} \simeq \frac{\dot{h}}{b} \tag{2}$$

where $\dot{h}$ is the mean front velocity and b the height of the microchannel, which is seen in Fig. 1.

We first solve the Navier-Stokes equation inside the microchannel. Since the microchannel has a rectangular shape we define the velocity field in Cartesian coordinates. Due to the geometry and the low size of the experimental setup, the velocity only has an x component, and it only depends on the z coordinate. This is

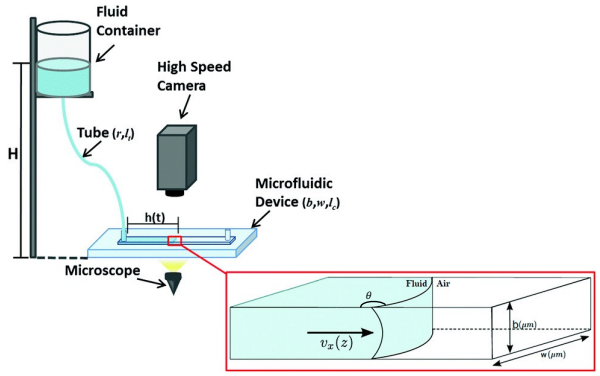

FIG. 1: Schematic image of the experimental setup used in the measurements of the pressure and the velocity of the mean fluid front. Extracted from Fig 1 of Trejo [7].

expressed as $\vec{v} = v_x(z)\,\hat{x}$, in Cartesian coordinates. The velocity field should depend on y and z coordinates because there is a front interface curvature due to capillary pressure, but since $b/w \ll 1$ we only consider the change in velocity with z.

$$F = \tau = \eta\left(\frac{dv_x}{dz}\right) = \eta\,\dot{\gamma} \tag{3}$$

This force is related to the tangential shear stress τ (note the difference with axial stress σ), since we are addressing the force applied tangentially to a differential layer of fluid.

We first need to start on the basis of Cauchy momentum equation for an incompressible fluid ($\vec{\nabla}\cdot\vec{v} = 0$):

$$\rho\,\frac{D\vec{v}}{Dt} = -\vec{\nabla}p + \vec{\nabla}\cdot\vec{\tau} \tag{4}$$

where ρ is the density of the fluid and $\vec{\nabla}p$ the pressure gradient.

Since we are in a low Reynolds number regime ($Re \approx 10^{-3}$) the stationary and convective terms equal to zero. Then we are left with $\vec{\nabla}p = \vec{\nabla}\cdot\vec{\tau}$, which can be written as (in Einstein notation):

$$\frac{\partial p}{\partial x_i} = \frac{\partial}{\partial x_j}\left(\tau_{ij}\right) \tag{5}$$

The stress tensor τ_{ij} (which is symmetrical) for an incompressible fluid is expressed as:

$$\tau_{ij} = \eta\left(\frac{\partial v_i}{\partial x_j} + \frac{\partial v_j}{\partial x_i}\right) \tag{6}$$

Since we only have an x component for the velocity field (only depending in z) we derive the shear tensor Eq. (6), considering $i = x$ and $j = x, y, z$:

$$\frac{\partial}{\partial x_j}\left(\tau_x\right) = \frac{\partial}{\partial x}\left[2\eta\frac{\partial v_x}{\partial x}\right] + \frac{\partial}{\partial y}\left[\eta\left(\frac{\partial v_x}{\partial y} + \frac{\partial v_y}{\partial x}\right)\right] + \\ + \frac{\partial}{\partial z}\left[\eta\left(\frac{\partial v_x}{\partial z} + \frac{\partial v_z}{\partial x}\right)\right] \tag{7}$$

Since $\frac{\partial v_x}{\partial z}$ is the only non-zero term we are left with an Stokes equation for fluids whose viscosity is shear-dependant:

$$\frac{\partial}{\partial z}\left(\eta\,\dot{\gamma}\right) = \frac{\partial p}{\partial x} \tag{8}$$

Since the velocity only has an x component, from now on we will be considering that $v \equiv v_x$, for the sake of simplicity.

The pressure gradient can be expressed as a function of the fluid mean front position, $h(t)$, and the pressure drop along the system, Δp:

$$\frac{\partial}{\partial z}\left(\eta(z)\cdot\dot{\gamma}(z)\right) = \frac{\Delta p}{h} \tag{9}$$

The pressure drop have three main contributions: the hydrostatic pressure p_{hyd} (which serves as the main pressure source to keep the front moving forward), the capillary pressure Δp_{YL} (which is related to the curvature of the fluid front) and the pressure drop along the microtube Δp_t (since we have a viscous fluid):

$$\Delta p = p_{hyd} - \Delta p_{YL} - \Delta p_t \tag{10}$$

The hydrostatic pressure can be assumed as constant in time since the height difference to get the microchannel completely filled is negligible (the container area is very big) [8].

The capillary pressure can be calculated with:

$$\Delta p_{YL} = 2\,\tau\cos\theta\left(\frac{1}{b} + \frac{1}{w}\right) \tag{11}$$

where θ is the contact angle between the fluid front and the microchannel wall (see Fig. 1), τ is the surface tension of the fluid and w is the width of the microchannel.

Substituting Eq. (1) in Eq. (9) and integrating we obtain the shear rate:

$$\dot{\gamma} = \left(\frac{z}{m}\frac{\Delta p}{h}\right)^{\frac{1}{n}} \tag{12}$$

which depends on h (therefore depends also on time). In order to compute the integration constant we have considered that the shear rate is 0 at the $z = 0$ plane as boundary conditions. Integrating Eq. (12) we get the velocity of the fluid as a function of z:

$$v(z) = \frac{n}{1+n}\left(\frac{\Delta p}{mh}\right)^{\frac{1}{n}}\left[z^{\frac{1}{n}+1} - \left(\frac{b}{2}\right)^{\frac{1}{n}+1}\right] \tag{13}$$

To calculate Eq. (13) we have considered non-slip boundary conditions because the fluid have velocity equal to zero relative to the wall, so $v(z = \pm b/2) = 0$.

In order to relate the velocity of the fluid with the flow we need to compute the total flow through the microchannel Q_m using Eq. (13):

$$Q_m = \int_S v(z)\,dS = w\int_{-\frac{b}{2}}^{\frac{b}{2}} v(z)\,dz = 2w\int_0^{\frac{b}{2}} v(z)\,dz = \\ = 2w\left(\frac{n}{1+2n}\right)\left(\frac{\Delta p}{mh}\right)^{\frac{1}{n}}\left(\frac{b}{2}\right)^{\frac{1}{n}+2} \tag{14}$$

Since the flow through the microchannel is also $Q_m = bw\dot{h}$ we are able to express the total pressure drop (which can be obtained through measurements) arranging Eq. (14) like:

$$\Delta p = \left(\frac{1+2n}{n}\right)^n \left(\frac{2}{b}\right)^{n+1} mh\dot{h}^n \tag{15}$$

We first need to compute the pressure drop through the micro-tube. Starting again from Eq. (5) and Eq. (6), but now using cylindrical coordinates and taking into account the new scale factors because the geometry of the micro-tube is different from the microchannel. The velocity only has a z component (due to mass conservation and that the fluid is incompressible) and only depends on the radius which is expressed as $\vec{v} = v_z(r)\,\hat{z}$. The stress tensor for the z component in cylindrical coordinates is:

$$\frac{\partial}{\partial x_j}(\tau_z) = \frac{\partial}{\partial z}\left[2\eta\frac{\partial v_z}{\partial z}\right] + \frac{1}{r}\frac{\partial}{\partial \phi}\left[\eta\left(\frac{\partial v_\phi}{\partial z} + \frac{1}{r}\frac{\partial v_z}{\partial \phi}\right)\right] + \\ + \frac{1}{r}\frac{\partial}{\partial r}\left[r\,\eta\left(\frac{\partial v_z}{\partial r} + \frac{\partial v_r}{\partial z}\right)\right] \tag{16}$$

Given that the only non-zero term is $\frac{\partial v_z}{\partial r}$ we are left with:

$$\frac{1}{r}\frac{\partial}{\partial r}\left(r\,\eta\,\frac{\partial v_z}{\partial r}\right) = \frac{\Delta p_t}{l_t} \tag{17}$$

where we directly substituted $\frac{\partial p}{\partial z} = \frac{\Delta p_t}{l_t}$, being l_t the length of the micro-tube.

Following a similar procedure than before we integrate Eq. (17) and obtain the velocity profile:

$$v_z(r) = \left(\frac{\Delta p_t}{2ml_t}\right)^{\frac{1}{n}} \left(\frac{n}{1+n}\right)\left[r^{\frac{1}{n}+1} - r_t^{\frac{1}{n}+1}\right] \tag{18}$$

where r_t is the radius of the micro-tube. In Eq. (18) we also considered non-slip boundary conditions $v_z(r = r_t) = 0$. Now we compute the flow through the micro-tube Q_t:

$$Q_t = 2\,\pi\left(\frac{\Delta p_t}{2ml_t}\right)^{\frac{1}{n}} \left(\frac{n}{1+n}\right)\int_0^{r_t}\left[r^{\frac{1}{n}+1} - r_t^{\frac{1}{n}+1}\right] r\,dr = \\ = \left(\frac{\Delta p_t}{2ml_t}\right)^{\frac{1}{n}} \left(\frac{n}{1+3n}\right)\pi r_t^{\frac{1}{n}+3} \tag{19}$$

Since $Q_t = \pi r_t^2 v_t$ (being v_t the mean velocity through the micro-tube) we can obtain Δp_t substituting in Eq. (19):

$$\Delta p_t = 2\,m\,l_t\,v_t^n \left(\frac{1+3n}{n}\right)^n \left(\frac{1}{r_t}\right)^{n+1} \tag{20}$$

From flow conservation ($Q_t = Q_m$) we can relate the velocities inside the micro-tube and inside the microchannel:

$$\pi r_t^2 v_t = bw\dot{h} \tag{21}$$

By substituting Eq. (10), Eq. (20) and Eq. (21) into Eq. (15) we finally obtain the mean front velocity:

$$\dot{h}^n = \frac{p_{hyd} - \Delta p_{YL}}{\left[\left(\frac{1+2n}{n}\right)^n \left(\frac{2}{b}\right)^{n+1} m\,h + \frac{2\,m\,l_t}{r_t^{n+1}}\left(\frac{b\,w}{\pi\,r_t^2}\left(\frac{1+3n}{n}\right)\right)^n\right]} \tag{22}$$

In Eq. (22) we have a very complex expression, but we can reduce it by considering the height of the microchannel b. In the denominator we have two terms: the first term is $\propto b^{-(n+1)}$ while the second one is $\propto b^n$. In order to get rid of the h dependence (since its difficult to measure the front position along time) we need a big value of b. As long as the height of the microchannel is high enough, the first term of the denominator will be much smaller than the second one and it can be omitted. This happens because the resistance in the micro-tube is higher than in the microchannel [7]. With this approximation, we are left with a much simpler expression of Eq. (22).

Given that we neglected the h dependant term, we can assume that the velocity of the fluid mean front $\dot{h}$ is constant through the microchannel ($\dot{h} \neq \dot{h}(t)$). From Eq. (22) we are left with:

$$p_{hyd} - \Delta p_{YL} = \frac{2\,l_t}{r^{n+1}}\left[\frac{b\,w}{\pi\,r_t^2}\left(\frac{1+3n}{n}\right)\right]^n m\,\dot{h}^n \tag{23}$$

This equation will allow us to measure the m variable for any non-Newtonian fluid. With this value we will be able to calculate the viscosity of the fluid with Eq. (1).

III. EXPERIMENTAL METHOD

To obtain the viscosity of blood we need experimental data of the mean front velocity $\dot{h}$ for various pressure values P_{eff}. The measured pressure is labelled as effective pressure, P_{eff}, which we define as: $P_{eff} = p_{hyd} - \Delta p_{YL}$. So values of the height of the fluid column and the contact angle are needed. The mean front velocity and the contact angle are measured with the footage taken from a high speed camera on a microscope. By tracking the mean front position of the fluid and measuring the time between segments of the microchannel, the velocity of the fluid is computed.

By repeating the same measurements for different column heights we will obtain a qualitative plot of the viscosity depending on the shear rate applied. The experimental setup characteristics and parameters are shown in Table I.

Because the viscosity of blood is shear dependant we need to compute the flow consistency index m and the power law exponent n with Eq. (23). With the given experimental data we can plot P_{eff} versus $\dot{h}$ to obtain a graph like Fig. 2, however it is not viable to directly obtain the value of n with Eq. (23). By applying logarithms to both sides of the equation we get:

$$\log P_{eff} = n\,\log\dot{h} + \log K \tag{24}$$

TABLE I: Experimental setup conditions.

b	$350\,\mu$m
w	$1000\,\mu$m
r_t	$127\,\mu$m
l_t	$0,43$ m
τ	$0,0612$ N/m
ρ	$1060\,\mathrm{kg/m^3}$

K is a constant defined as:

$$K = \frac{2\,l_t}{r^{n+1}} \left[\frac{b\,w}{\pi\,r_t^2} \left(\frac{1+3n}{n} \right) \right]^n m \tag{25}$$

Therefore plotting the logarithm of P_{eff} versus the logarithm of $\dot{h}$ and making a linear regression we can compute n (which equals the slope of the linear regression) and m (dividing the value of K by all the prefactor of m in Eq. (25)).

IV. EXPERIMENTAL RESULTS AND DISCUSSION

As mentioned in the introduction, we analyse experimental data from mice infected by *Plasmodium yoelii*-GFP transgenic line. This non-lethal parasite serves as a basis to understand *P. vivax* in the future, due to the similar structural changes that IRBCs suffer upon infection. The experimental data was measured by Aleix Elizalde and Claudia Trejo in 2017 and briefly analyzed in [9], not computing the viscosity of the samples.

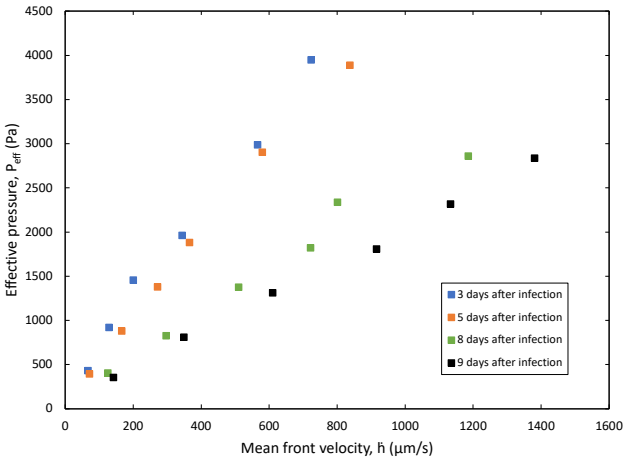

FIG. 2: Effective pressure as a function of mean front velocity for the *P. yoelii* infected mice blood.

The experimental data comes from four mice that were infected by *Plasmodium yoelii*-GFP transgenic line and were killed 3, 5, 8 and 9 days after the infection. This was made in order to analyse the change in blood rheological properties along time.

Working with the experimental setup described earlier we obtain the mean front velocity $\dot{h}$ for every pressure applied P_{eff}. Using the equations described before we obtain the viscosity and we can plot the viscosity versus the shear rate extract useful information.

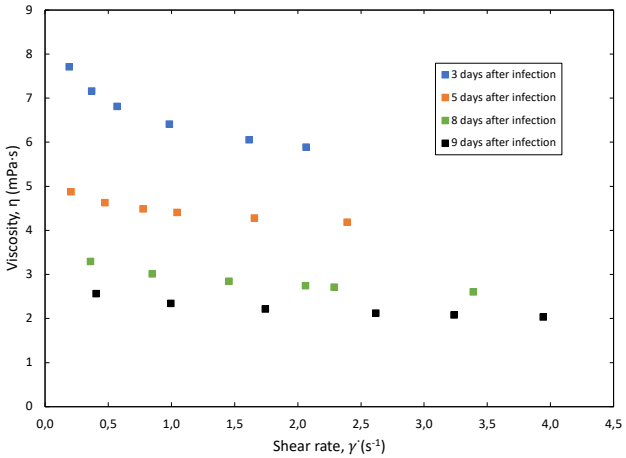

FIG. 3: Viscosity as a function of shear rate for the *P. yoelii* infected mice blood.

As seen in Fig. 2, the slope of the curve decreases with infection time. Since the slope is related to the viscosity of the blood we will see a decrease in blood viscosity, which is noticeable in Fig. 3. These *P. yoelii* results have correlation with the recent studies of *P. vivax*. As the parasite mature the RBCs become more deformable [4], which can be seen in Fig. 3 if we directly relate the deformability of the RBCs with the viscosity of the blood.

We can also observe that in Fig. 3, the shear-thinning behaviour of blood is less noticeable as the infection progresses. This could happen due to the increase of deformability of the RBCs. Another cause could be the decrease of *rouleaux* formation because of the deformability changes. *Rouleaux* are aggregations of RBCs due to their unique biconcave discoid shape, and are the main cause of increased blood viscosity at low shear rates. Since *P. vivax* tends to enlarge the surface area, this might affect the number of *rouleaux* formed and consequently decrease the viscosity of blood at this lower shear rates.

More studies are needed to understand the structural and deformability changes in IRBCs by *P. vivax* in order to properly compare these changes with the viscosity of the blood.

Finally, the viscosity results of non-infected human blood extracted from [8] are shown in Fig. 4. Since mice and human blood has a similar hematocrit (*circa* 48%) we can approximately compare the viscosity values. We will consider the pink curve, as is the less aged blood sample with an hematocrit of 48%. The mice infected blood results we obtained have a lower value than the human blood results. The viscosity of the blood with 3

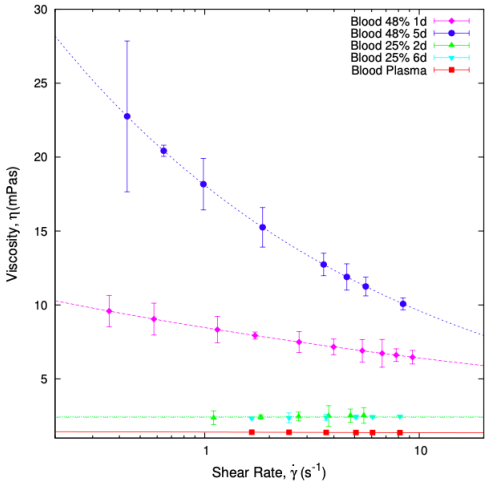

FIG. 4: Viscosity as a function of shear rate for the non-infected by malaria human blood. Plot extracted from Fig 9.4 of Trejo [8].

days after infection is lower than the human non-infected blood; the same happens for larger infection periods of time. This could be related to the higher deformability that RBCs undergo when infected by *P. vivax*, resulting in an overall decrease of blood viscosity as the disease advance.

V. CONCLUSIONS

We have successfully employed a mathematical model to calculate the viscosity of *P. yoelii* and non-infected blood for different shear rate values. A qualitative relation between the viscosity values and the already known viscoelastic changes in IRBCs is made with the aim of better comprehending the unusual behaviour of blood viscosity when infected by malaria.

My future objective is to inquire more deeply into the rheology of human blood, especially blood infected with malaria, working along Dra. Aurora Hernández Machado and Dr. Hernando del Portillo. A focus on *P. vivax* and *P. falciparum* is required to better understand their effects on blood viscoelastic properties and advance towards a faster diagnosis, a more effective cure and the eradication of this disease.

Acknowledgments

I would like to express my gratitude to Dra. Hernández Machado, who has been advising me throughout the whole semester and gave me this amazing opportunity to study on this topic; her enthusiasm and positive attitude kept me always moving forward.

I also want to thank my partner, my family and my friends, who always support and encourage me, especially in this busy and complicated semester.

[1] Somer T, Meiselman HJ. "Disorders of blood viscosity", *Annals of Medicine*, Volume 25, Issue 1, pp. 31-39 (1993).
[2] WHO. "World malaria report 2017", Geneva: World Health Organization (2017).
[3] Jeanne R. Poespoprodjo et al. "Vivax Malaria: A Major Cause of Morbidity in Early Infancy", *Clinical Infectious Diseases*, Volume 48, Issue 12, pp. 1704-1712 (2009).
[4] Suwanarusk R, Cooke BM, Dondorp AM, Silamut K, Sattabongkot J, White NJ, Udomsangpetch R. "The deformability of red blood cells parasitized by Plasmodium falciparum and P. vivax", *J Infect Dis*, Volume 189, Issue 2, pp. 190-194 (2004).
[5] Oihane Ezama Espina. "Experimental study of red blood cells infected by Malaria: a microdevice", Master Thesis, *Universitat de Barcelona* (2017).
[6] Rigat-Brugarolas LG, Elizalde-Torrent A, Bernabeu M, De Niz M, Martin-Jaular L, Fernandez-Becerra C, Homs-Corbera A, Samitier J, del Portillo HA. "A functional microengineered model of the human splenon-on-a-chip", *Lab Chip*, Volume 14, Issue 10, pp. 1715-1724 (2014).
[7] Trejo-Soto C, Costa-Miracle E, Rodriguez-Villareal I, Cid J, Castro M, Alcorcón T, Hernández-Machado A. "Front microrheology of the non-Newtonian behaviour of blood: scaling theory of erythrocyte aggregation by aging", *Soft Matter*, Volume 13, Issue 16, pp. 3042-3047 (2017).
[8] Claudia A. Trejo Soto. "Front Microrheology of Biological Fluids", PhD Thesis, *Universitat de Barcelona* (2016).
[9] Aleix Elizalde Torrent. "The role of the spleen in Plasmodium vivax malaria", PhD Thesis, *Universitat de Barcelona* (2018).